SCIENTIFIC REPORTS

OPEN

SUBJECT AREAS:
SYNTHESIS
MATERIALS CHEMISTRY
TWO-DIMENSIONAL MATERIALS
NANOSCALE MATERIALS

Received
16 January 2013

Accepted
25 June 2013

Published
12 July 2013

Correspondence and requests for materials should be addressed to Q.Y.L. (qylu@nju.edu.cn) or F.G. (fgao@nju.edu.cn)

Two-Dimensional β-MnO_2 Nanowire Network with Enhanced Electrochemical Capacitance

Chengzhen Wei[1,2], Huan Pang[1,2], Bo Zhang[2], Qingyi Lu[1], Shuang Liang[1] & Feng Gao[2]

[1]State Key Laboratory of Coordination Chemistry, Coordination Chemistry Institute, Nanjing National Laboratory of Microstructures, School of Chemistry and Chemical Engineering, Nanjing University, Nanjing 210093, P. R. China, [2]Department of Materials Science and Engineering, Nanjing University, Nanjing 210093, P. R. China.

Conventional crystalline β-MnO_2 usually exhibits poor electrochemical activities due to the narrow tunnels in its rutile-type structure. In this study, we synthesized a novel 2D β-MnO_2 network with long-range order assembled by β-MnO_2 nanowires and demonstrated that the novel 2D β-MnO_2 network exhibits enhanced electrochemical performances. The 2D network is interwoven by crossed uniform β-MnO_2 nanowires and the angle between the adjacent nanowires is about 60°. Such a novel structure makes efficient contact of β-MnO_2 with electrolyte during the electrochemical process, decreases the polarization of the electrode and thus increases the discharge capacity and high-rate capability. The specific capacitance of the obtained 2D β-MnO_2 network is 453.0 F/g at a current density of 0.5 A/g.

Network-like structures with one dimensional (1D) nanostructures (nanowires, nanorods or nanotubes) as building blocks can function as both devices and interconnections, and thus are expected to play key roles in the production of the next generation of nano-devices[1]. In the past years, several groups have reported the synthesis of two-/three-dimensional (2D/3D) arranged nanowire networks. Through a chelation-deposition-epitaxy growth mechanism, 2D CdS nanowire networks were obtained with the assistance of BiI_3 flake template[2]. Wang et al. reported the preparation of metal and semiconductor nanowire network thin films through electrochemical processes using pore structures as a template[3]. These nanowire-based networks were synthesized by template methods (such as BiI_3 flake template or mesoporous silica film template) and the processes needed complicated multi-steps to remove the templates or selectively etch the flake precursor in appropriate solvents, which would make the products impure and limit their applications. Thermal evaporation and deposition routes at high temperatures were reported for the synthesis of 2D/3D arranged nanowire networks of WO_3,[4] InAs[5] and PbSe[6]. But the high temperatures limit its applications for extensive synthesis of 2D or 3D networks. Recently, low-temperature chemical methods have been reported to fabricate network structures with high order. With the assistance of biomolecules, highly ordered snowflake-like structures made up of bismuth sulfide nanorods were obtained under microwave-hydrothermal conditions[7]. 2D disc-like Bi_2S_3 nanorod networks were prepared via a novel topotactic transformation process, which involves the formation of intermediate BiOCl discs and their subsequent chemical transformation into disc-like Bi_2S_3 networks[8]. Although some successes have been achieved, there is still a big challenge for materials scientists to fabricate network nanostructures with regular long-range order through a mild and simple method.

Energy consumption/production relying on the combustion of fossil fuels results in CO_2 emissions and is predicted to have an adverse effect on world economy and ecology[9,10]. Consequently, to develop alternative energy sources has attracted intense interests and many efforts have been focus on the efficient storage of electrical energy generated from intermittent energy sources such as wind, solar, wave and tidal powers[11–15]. Supercapacitors, also known as electrochemical capacitors, exhibit many advantages such as high powder capability, long cycle life, fast charging and discharging rate[16–18]. They have attracted tremendous attention and been thought to be possible candidates for next generation of energy storage systems[19–20]. The decisive task for constructing a supercapacitor is exploring good electrode materials that meet the desired requirements. During the past years, attentions have been paid to cheap metal oxides, expected to serve as economical alternatives for hydrous RuO_2, the state-of-the-art EC metal oxide but expensive and poisonous[21–24]. Manganese oxides, as transition metal oxides, have been investigated as electrode materials[25–27]. MnO_2 has several polymorphs including α, β, γ, δ, λ and ε forms, among which β-MnO_2 has best thermodynamic stability and is easy to be obtained. Compared to the other MnO_2,

β-MnO_2 has a rutile-type tetragonal symmetry ($P4_2/mnm$) with a distorted hexagonal-close packed oxygen array, where edge-sharing MnO_6 octahedra stacks and forms 1 × 1 (0.23 nm × 0.23 nm) tunnels[28]. β-MnO_2 received much attention in lithium batteries and showed good performances[29–31]. However, few investigations have been concentrated on the utilization of β-MnO_2 for electrochemical capacitors since the narrowest (1 × 1) tunnel in its structure makes it difficult for ions to diffuse into bulk upon electrochemically intercalating, resulting in that conventional crystalline β-MnO_2 usually exhibits poor electrochemical activities[29,30]. Up to now, the performances obtained using β-MnO_2 as electrode materials achieved unsatisfactory results[32,33]. Therefore, further improvement of the desired electrochemical performances is necessary. In this work, we successfully synthesized a 2-D β-MnO_2 network structure with long-range order assembled by β-MnO_2 nanowires through a mild solution method and demonstrated that the novel 2-D β-MnO_2 network structure show enhanced electrochemical performances. The specific capacitance of the obtained 2D β-MnO_2 network is 453.0 F/g at a current density of 0.5 A/g. This value is much higher than those in the previous reports[32,33]. We also found that the 2D β-MnO_2 network shows better electrochemical performances compared to α-MnO_2 electrode materials[34,35]. Furthermore, the 2D β-MnO_2 network exhibit excellent cyclic performance with ca. 97% capacity retention at 2.5 A/g after 1800 cycles, which may provide promising potential to be a electrode material for supercapacitors.

Results

The 2D β-MnO_2 nanowire networks were achieved by mixing $(NH_4)_3PO_4$ aqueous solution and hydrolysis solution of $Mn(NO_3)_2$, followed by incubation at 220 °C for 6 hours under hydrothermal conditions. The X-ray diffraction (XRD) pattern of the obtained product is given in Fig. 1. All of the reflection peaks can be indexed to tetragonal β-MnO_2 (JCPDS card No. 24-0735). No peaks of any other phases are detected, indicating the high purity of the product. Fig. 2 presents typical scanning electron microscopy (SEM) images of the obtained sample. The low magnification SEM image in Fig. 2a shows that the predominant product is micrometer-sized 2D networks. Indeed, the yield of the 2D networks is very high based on the SEM investigations and the process is reproducible. An enlarged image in Fig. 2b confirms that the 2D network structures are like nanofabrics interweaving by many nanowires with long-range order and the ordered nanowire arrays can be seen at the edge of 2D networks. From Fig. 2c, we can see the detailed structure of 2D network structures. The 2D network is made of crossed nanowires and the nanowires constituting the nanofabrics are uniform with a diameter about 20 nm and the angle between the adjacent nanowires is about 60°. The thickness of 2D network structures is uniform as shown in Fig. 2d. It can be also found from Fig. 2d that the 2D β-MnO_2 network is flexible.

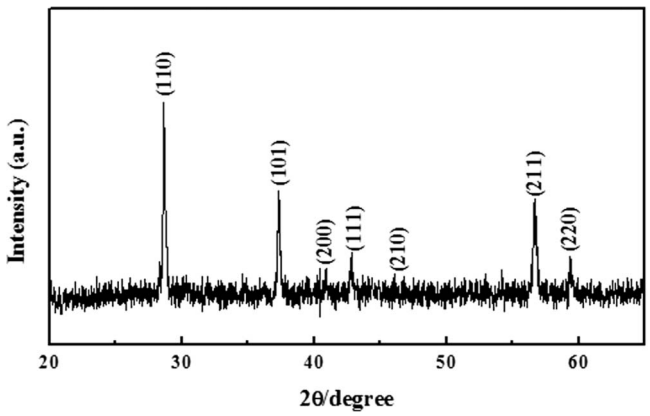

Figure 1 | XRD pattern of the as-prepared product.

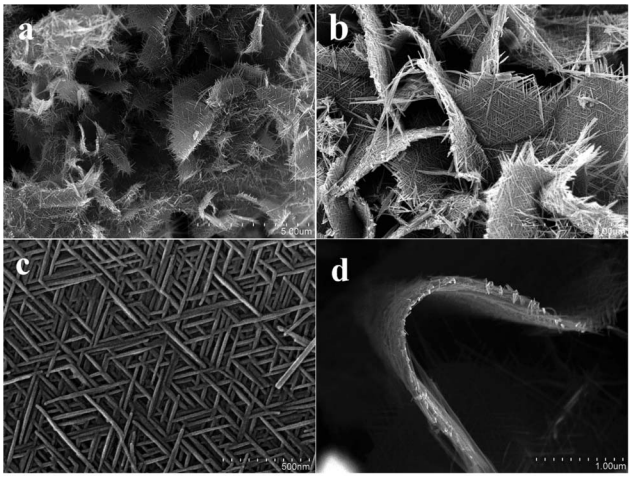

Figure 2 | SEM images with different magnifications of the obtained β-MnO_2 network.

The product was further characterized by transmission electronic microscopy (TEM) and the TEM images presented in Fig. 3a and b confirms that the obtained product is of 2D network structure consisting of crossed nanowires with long-range order and the nanowires constituting the network are uniform with a diameter about 20 nm. The crystalline structure of the β-MnO_2 nanowires in the 2D networks was investigated by selected area electron diffraction (SAED) and high-resolution TEM (HRTEM) investigations. The SAED pattern corresponding to the whole 2D interwoven network shown in Fig. 3a is presented in Fig. 3c, which exhibits orderly arranged spots with a hexagonal-like symmetry, reflecting that the β-MnO_2 nanowires are interweaved into the network in a hexagonal symmetry with the angle between the adjacent nanowires of about 60°. The diffraction spots in this pattern are large and strong. Fig. 3d

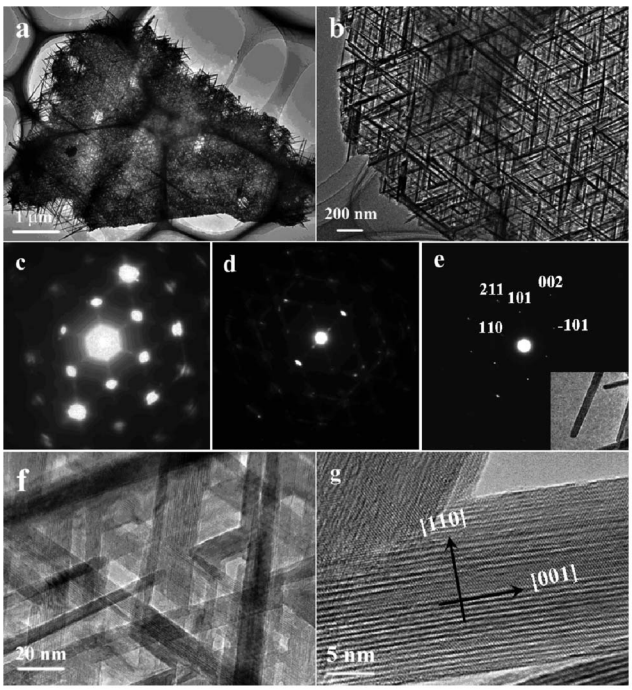

Figure 3 | (a, b) TEM images; (c~e) SAED patterns and (f, g) HRTEM images of the obtained β-MnO_2 network.

shows a SAED pattern of edge part of the network presented in Fig. 3a, displaying several sets of diffraction spots that comes from different β-MnO_2 nanowires. By comparing the two SAED patterns in Fig. 3c and d, it can be suggested that the strong diffraction spots in Fig. 3c might result from the overlap of many sets of diffraction spots from the long range network of β-MnO_2 nanowires. An SAED pattern of a single nanowire was taken and shown in Fig. 3e (inset in Fig. 3e is the corresponding TEM image of the single nanowire). From Fig. 3e, only one set of diffraction spots can be observed and by comparing the three SAED patterns, it can be concluded that the nanowires might adopt a common growth direction and be interweaved in a hexagonal symmetry. The two diffraction spots in Fig. 3e perpendicular to each other can be indexed to (110) and (002) respectively, indicating the single nanowire has a growth direction of [001]. Fig. 3f show a HRTEM image of the network and clear lattice fringes can be observed, revealing that all the crossed nanowires exhibit the same crystallographic orientation. A typical HRTEM image of an individual nanowire (Fig. 3g) exhibits clear lattice fringes corresponding to the {110} planes and suggests that the nanowire is single-crystalline with [001] growth direction, which is consistent with the results from the SAED characterizations.

The growth process of the 2D β-MnO_2 nanowire networks was studied by investigating the phase, morphology and structure of the products obtained at 220 °C for different reaction times. After the addition of $(NH_4)_3PO_4$ solution to the hydrolysis solution of $Mn(NO_3)_2$, a white precipitate formed. The corresponding XRD pattern shown in Supplementary Fig. S1a suggests that the precursor is $Mn_3(PO_4)_2 \cdot 3H_2O$ (JCPDS Card No. 03-0426). From Supplementary Fig. S2a, the obtained $Mn_3(PO_4)_2 \cdot 3H_2O$ has a plate-like structure. After 1 h of reaction at 220 °C, there are some diffraction peaks corresponding to β-MnO_2 appeared, indicating a partial transformation from $Mn_3(PO_4)_2 \cdot 3H_2O$ into β-MnO_2 (See Supplementary Fig. S1b). After 4 h of reaction at 220 °C, it can be seen from Supplementary Fig. S2c that the original solid plates have evolved into disc-like nanowire networks. However, the XRD result (Supplementary Fig. S1c) shows that some peaks corresponding to the precursor are still evident after 4 h reaction, which suggests the completed transformation from $Mn_3(PO_4)_2 \cdot 3H_2O$ into β-MnO_2 needs longer reaction time. A further prolongation of the reaction time to 6 h results in the formation of pure 2D β-MnO_2 nanowires networks.

The performances of the obtained 2D β-MnO_2 network as an EC electrode material were investigated in this study. For comparison, two other β-MnO_2 structures have also been synthesized according to the previous reports[36,37]. Their SEM images are shown in Supplementary Fig. S3. For convenience, the three samples are noted as M-1, M-2 and M-3, respectively. Fig. 4a displays the cyclic voltammetry (CV) curves of the β-MnO_2 nanowire network electrode at scan rates of 2, 5, 10, 12, 25 and 50 mV/s with potential windows ranging from 0 to 0.8 V versus $Hg/HgCl_2$ in 1 M Na_2SO_4 aqueous solution. The shapes of these curves are quasi-rectangular, indicating the ideal electrical double-layer capacitance behaviors and fast charging/discharging process characteristics. In the CV tests the β-MnO_2 involved redox reactions as Mn atoms were converted into higher/lower valence states, which were induced by intercalation/extraction of protons (H_3O^+) or alkali cations (Na^+) into/out of the channels of the β-MnO_2 network. To demonstrate the electrochemical performance benefits of the β-MnO_2 network structures, CV tests were also performed on M-2 and M-3, as shown in Supplementary Fig. S4. Although they display similar CV shapes, the separations between leveled anodic and cathodic currents at the same scan rates are much smaller than those of the β-MnO_2 network, indicating smaller specific capacitances. The specific capacitance calculated from the CV curve at the scan rate of 2 mV/s of the β-MnO_2 network is 381.2 F/g, while those of M-2 and M-3 are only 30.3 and 24.2 F/g, respectively. Fig. 4b shows the constant-current galvanostatic (GV) charge/discharge curves of the as-prepared β-MnO_2 network at different current densities. The charge/discharge curves show a symmetric nature, indicating that the material has a good electrochemical capacitive characteristics and superior reversible redox reaction. This symmetric nature of the charge/discharge curves can be maintained even at a low density of 0.5 A/g. The specific capacitances derived from the discharge curves at different current densities are shown in Fig. 4c along with those of M-2 and M-3. The specific capacitance of β-MnO_2 network structure material at the current density of 0.5 A/g was calculated to be 453.0 F/g, much larger than those of M-2 and M-3 (35.0 F/g and 30.0 F/g) and bulk β-MnO_2 materials. It is also much higher than those previously reported[32,33] and α-MnO_2 electrode materials[34,35]. Specific energy and specific power are the two key factors for evaluating the power applications of electrochemical supercapacitors. Fig. 4d shows the Ragone plot for the β-MnO_2 materials electrode at the potential window of 0.8 V in 1 M Na_2SO_4 aqueous solution. The specific energy decreases from 34.1 to 22.0 Wh/kg, while the specific power increases from 0.8 to 8.8 kW/kg as the galvanostatic (GV) charge/discharge current increases from 1 to 11 A/g. These values are much higher than those of M-2 and M-3. Another important requirement for supercapacitor applications is cycling capability or cycling life. The cycling life tests over 1800 cycles for the β-MnO_2 networks electrode at a current density of 2.5 A/g were carried out using constant current galvanostatic (GV) charge/discharge cycling techniques. Fig. 4e shows the specific capacitance retention of the β-MnO_2 materials electrode as a function of charge/discharge cycling numbers. The β-MnO_2 network electrode shows only 3.0% loss in the specific capacitance after 1800 charge-discharge cycles, while those of M-2 and M-3 can't retain 50% of their first specific capacitances.

Discussion

The two-dimensional (2D) β-MnO_2 networks with long-range order assembled by crossed single-crystalline β-MnO_2 nanowires were synthesized via a 2D-template-transformation process, which involves the formation of intermediate $Mn_3(PO_4)_2 \cdot 3H_2O$ plate-like structures and their subsequent transformation into β-MnO_2 networks. The electrochemical studies show that compared to M-2 and M-3 processing very low capacity and poor cycling capability, the as-prepared β-MnO_2 network exhibits enhanced electrochemical activities with high specific capacitance and excellent cyclic performances. The electrochemical activities of the as-prepared β-MnO_2 network should be related to its special network structure. Although the size of the as-prepared β-MnO_2 network is in micrometer scale as the other two samples, it is made of crossed nanowires, which creates porous channels and results in an increase of surface area. The porous channels and increase surface areas enable effective electrolyte transport and active site accessibility, leading to the enhanced specific capacitance.

To further understand the electrode kinetics, the activation energies of the β-MnO_2 electrodes were estimated by electrochemical impedance spectra (EIS). Fig. 4f and Supplementary Fig. S5a, b show the EIS of the electrodes of M-1, M-2 and M-3 at different temperatures. The EIS data can be fitted by an equivalent circuit consisting of a bulk solution resistance R_s, a charge-transfer R_{ct}, a pseudocapacitive element C_p from redox process of MnO_2, and a constant phase element (CPE) to account for the double-layer capacitance (The equivalent circuit diagram is shown in Supplementary Fig. S5c). Then, the exchange current (i_0) and the apparent activation energy (E_a) for the intercalation of cations can be calculated by $i_0 = RT/nFR_{ct}$ and the Arrhenius equation $i_0 = A\exp(-E_a/RT)$, respectively, where A is a temperature-independent coefficient, R is the gas constant, T is the absolute temperature, n is the number of transferred electrons, and F is the Faraday constant. The activation energies of M-1, M-2 and M-3 are calculated to be 21.06, 34.08 and 40.01 kJ/mol, respectively. The lowest activation energy of M-1 indicates the shortest diffusion route for cation intercalation. This enhanced kinetics might be due to the fact that the BET surface area of M-1 (15.3 m^2/g) is

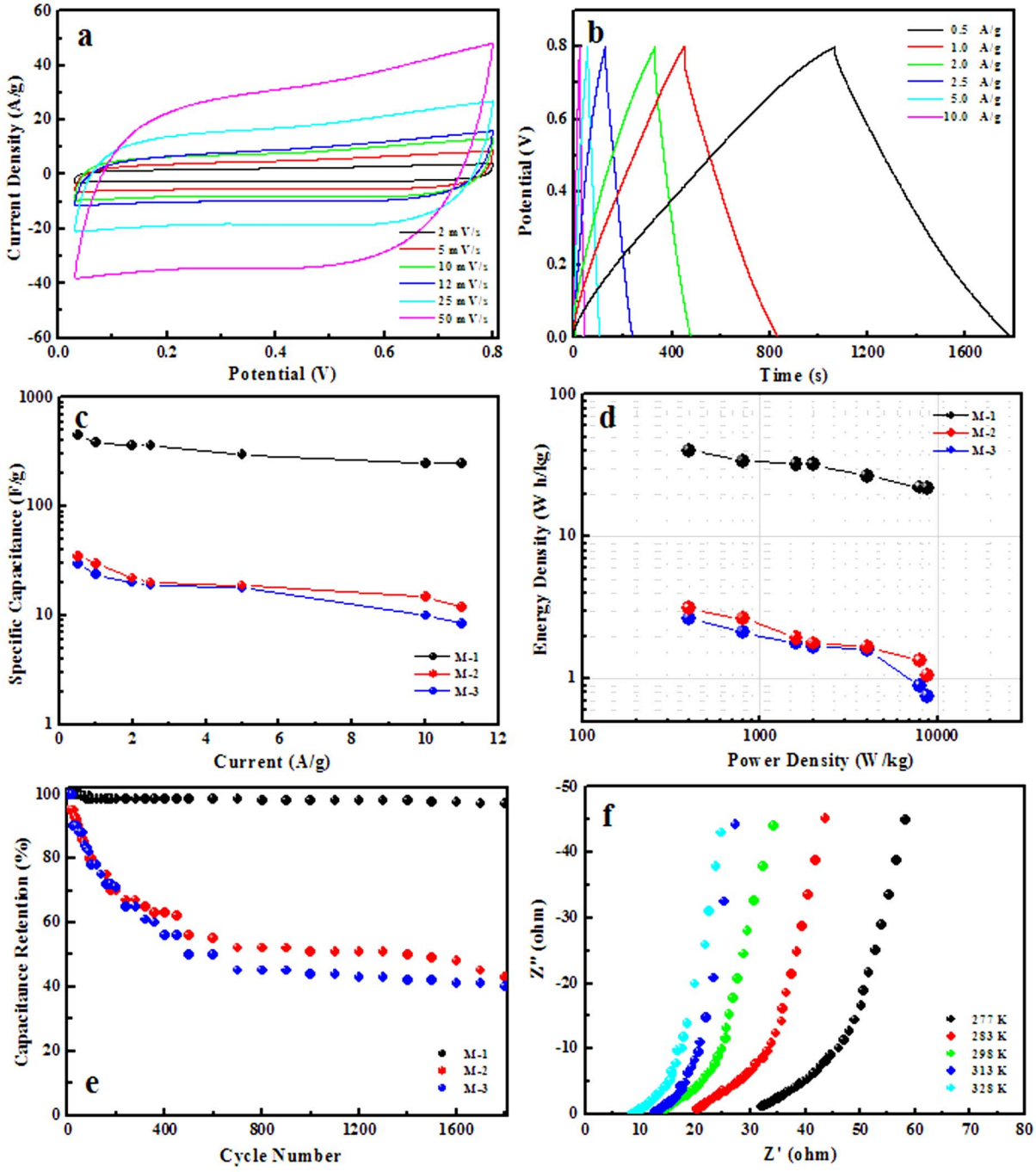

Figure 4 | (a) CV curves of the β-MnO_2 network electrode; (b) GV constant current charge/discharge curves of the β-MnO_2 network electrode at different current densities; (c) Specific capacitances of M-1, M-2 and M-3 at different current densities; (d) Ragone plots of the estimated specific energy and specific power of M-1, M-2 and M-3 at various charge/discharge rates; (e) Charge/discharge cycling tests of M-1, M-2 and M-3 at the current density of 2.5 A/g; (f) Electrochemical impedance spectra of the β-MnO_2 network electrode at different temperatures.

much larger than those of M-2 and M-3 (7.2, and 8.3 m^2/g), making the efficient contact of the network with the electrolyte. The special network structure leads to the fact that electrolyte can flood into pores of the network structure and its inner surface is available for ion diffusion. This surface/interface character decreases the polarization of the electrode and thus increases the discharge capacity and high-rate capability. Moreover, the porous 2D network is able to provide an extra space for the diffusion of electrolyte and reduce the stress caused by the cracking of the structure during the discharge process and, thus, suppress the degradation of the electrode[38].

In summary, unique 2D β-MnO_2 nanowire networks were synthesized through a solution approach avoiding the extreme reaction conditions and the assistance of templates/substrates. It was revealed that these superstructures were formed by the preferential growth of [001]-oriented β-MnO_2 nanowires. The obtained 2D β-MnO_2 nanowire networks show high specific capacitance, high-energy density, high-power density and long-term life as electrocapacitor electrode materials. The results suggest that such 2D β-MnO_2 nanowire networks supercapacitor electrode would be promising for next generation high-performance supercapacitors.

Methods

Preparation of β-MnO_2 nanowire networks. $(NH_4)_3PO_4$ (0.2 g) and distilled water (25 mL) were mixed with a hydrolysis solution of 50% $Mn(NO_3)_2$ (2 mL) and then

were maintained at 220 °C for 6 hours under hydrothermal conditions. The products were collected, washed three times with deionized water, and dried in air.

Characterizations. The structure of the as-obtained samples was characterized by X-ray powder diffractometer (Bruker D8 Advance) with Cu K_α radiation (λ = 0.15406 nm). Scanning electron microscopy (SEM) images of the as-obtained samples were observed by a Hitachi S-4800 field-emission scanning electron microscope (FE-SEM) at an acceleration voltage of 10.0 kV. Transmission electron microscopy (TEM) images and the corresponding selected area electron diffraction (SAED) patterns were taken on the JEM-2100 transmission electron microscope at an acceleration voltage of 200 kV.

Electrochemical Measurements. The working electrodes of electrochemical capacitors were formed by mixing the prepared powder with 15 wt% acetylene black and 5 wt% poly-(tetrafluoroethylene) (PTFE) binder of the total electrode mass. A small amount of distilled water was then added to those mixtures to make them more homogeneous. The mixtures were pressed onto nickel foam current collectors (1.0 × 1.0 cm^2) to fabricate electrodes. The typical loaded mass of electrode material was of 3–5 mg. All electrochemical measurements were done in a three-electrode experimental setup. Platinum foil with the same area as the working electrode and a saturated calomel electrode (SCE) were used as the counter and reference electrodes, respectively. All the electrochemical measurements were carried out in 1 M Na_2SO_4 aqueous electrolyte by using a CHI 660D electrochemical workstation (CHI Instruments).

1. Huang, Y. *et al*. Logic gates and computation from assembled nanowire building blocks. *Science* **294**, 1313–1317 (2001).
2. Li, H. Y. & Jiao, J. High-yield two-dimensional CdS nanowire networks synthesized by a low-temperature chemical method. *Chem. Mater.* **20**, 3770–3777 (2008).
3. Wang, D. H. *et al*. Metal and semiconductor nanowire network thin films with hierarchical pore structures. *Chem. Mater.* **18**, 4231–4237 (2006).
4. Zhou, J. *et al*. Three-dimensional tungsten oxide nanowire networks. *Adv. Mater.* **17**, 2107–2110 (2005).
5. Dick, K. A. *et al*. Position-controlled interconnected InAs nanowire networks. *Nano Lett.* **6**, 2842–2847 (2006).
6. Zhu, J. *et al*. Hyperbranched lead selenide nanowire networks. *Nano Lett.* **7**, 1095–1099 (2007).
7. Lu, Q. Y., Gao, F. & Komarneni, S. Biomolecule-assisted synthesis of highly ordered snowflakelike structures of bismuth sulfide nanorods. *J. Am. Chem. Soc.* **126**, 54–55 (2004).
8. Li, L. S. *et al*. Topotactic transformation of single-crystalline precursor discs into disc-like Bi_2S_3 nanorod networks. *Adv. Funct. Mater.* **18**, 1194–1201 (2008).
9. Winter, M. & Brodd, R. J. What are batteries, fuel cells, and supercapacitors?. *Chem. Rev.* **104**, 4245–4269 (2004).
10. Arunachalam, V. S. & Fleischer, E. L. Harnessing materials for energy. *MRS Bull.* **33**, 261–261 (2008).
11. Armand, M. & Tarascon, J. M. Building better batteries. *Nature* **451**, 652–657 (2008).
12. Tollefson, J. Car industry: Charging up the future. *Nature* **456**, 436–440 (2008).
13. Jacobson, M. Z. Review of solutions to global warming, air pollution, and energy security. *Energy Environ. Sci.* **2**, 148–173 (2009).
14. Baxter, J. *et al*. Nanoscale design to enable the revolution in renewable energy. *Energy Environ. Sci.* **2**, 559–588 (2009).
15. Subramanian, V., Zhu, H., Vajtai, R., Ajayan, P. M. & Wei, B. Hydrothermal synthesis and pseudocapacitance properties of MnO_2 nanostructures. *J. Phys. Chem. B* **109**, 20207–20214 (2005).
16. Simon, P. & Gogotsi, Y. Materials for electrochemical capacitors. *Nat. Mater.* **11**, 845–854 (2008).
17. Mai, L. Q. *et al*. Hierarchical $MnMoO_4/CoMoO_4$ heterostructured nanowires with enhanced supercapacitor performance. *Nat. Commun.* **2**, 381–385 (2011).
18. Jiang, H., Lee, P. S. & Li, C. 3D carbon based nanostructures for advanced supercapacitors. *Energy Environ. Sci.* **6**, 41–53 (2013).
19. Reddy, R. N. & Reddy, R. G. Synthesis and electrochemical characterization of amorphous MnO_2 electrochemical capacitor electrode material. *J. Power Sources* **132**, 315–320 (2004).
20. Conway, B. E. *Electrochemical Supercapacitors*, Kluwer Academic Plenum Publishers: New York, 1999.
21. Rakhi, R. B., Chen, W., Cha, D. & Alshareef, H. N. Substrate dependent self-organization of mesoporous cobalt oxide nanowires with remarkable pseudocapacitance. *Nano Lett.* **12**, 2559–2567 (2012).
22. Brezesinski, T., Wang, J., Tolbert, S. H. & Dunn, B. Ordered mesoporous α-MoO_3 with iso-oriented nanocrystalline walls for thin-film pseudocapacitors. *Nat. Mater.* **9**, 146–151 (2010).
23. Xu, M. W., Zhao, D. D., Bao, S. J. & Li, H. L. Mesoporous amorphous MnO_2 as electrode material for supercapacitor. *J. Solid State Electrochem.* **11**, 1101–1107 (2007).
24. Fischer, A. E., Pettigrew, K. A., Rolison, D. R., Stroud, R. M. & Long, J. W. Incorporation of homogeneous, nanoscale MnO_2 within ultraporous carbon structures via self-limiting electroless deposition: implications for electrochemical capacitors. *Nano Lett.* **7**, 281–286 (2007).
25. Yan, W. B. *et al*. Mesoporous manganese oxide nanowires for high-capacity, high-rate, hybrid electrical energy storage. *ACS Nano* **5**, 8275–8287 (2011).
26. Chen, S., Zhu, J. W., Wu, X. D., Han, Q. F. & Wang, X. Graphene oxide-MnO_2 nanocomposites for supercapacitors. *ACS Nano* **4**, 2822–2830 (2010).
27. Wu, Z. S. *et al*. High-energy MnO_2 nanowire/graphene and graphene asymmetric electrochemical capacitors. *ACS Nano* **4**, 5835–5842 (2010).
28. Thackeray, M. M. Manganese oxides for lithium batteries. *Prog. Solid State Chem.* **25**, 1–2 (1997).
29. Jiao, F. & Bruce, P. G. Mesoporous crystalline β-MnO_2—a reversible positive electrode for rechargeable lithium batteries. *Adv. Mater.* **19**, 657–660 (2007).
30. Luo, J. Y., Zhang, J. J. & Xia, Y. Y. Highly electrochemical reaction of lithium in the ordered mesoporosus β-MnO_2. *Chem. Mater.* **18**, 5618–5623 (2006).
31. Chen, W. M. *et al*. Controllable synthesis of hollow bipyramid β-MnO_2 and its high electrochemical performance for lithium storage. *ACS Appl. Mater. Interfaces* **4**, 3047–3053 (2012).
32. Devaraj, S. & Munichandraiah, N. Effect of crystallographic structure of MnO_2 on its electrochemical capacitance properties. *J. Phys. Chem. C* **112**, 4406–4417 (2008).
33. Zang, J. F. & Li, X. D. In situ synthesis of ultrafine β-MnO_2/polypyrrole nanorod composites for high-performance supercapacitors. *J. Mater. Chem.* **21**, 10965–10969 (2011).
34. Jiang, H., Zhao, T., Ma, J., Yan, C. Y. & Li, C. Z. Ultrafine manganese dioxide nanowire network for high-performance supercapacitors. *Chem. Commun.* **47**, 1264–1266 (2011).
35. Jiang, H., Ma, J. & Li, C. Z. Polyaniline-MnO_2 coaxial nanofiber with hierarchical structure for high-performance supercapacitors. *J. Mater. Chem.* **22**, 16939–16942 (2012).
36. Cheng, F. Y. *et al*. Facile controlled synthesis of MnO_2 nanostructures of novel shapes and their application in batteries. *Inorg. Chem.* **45**, 2038–2044 (2006).
37. Huang, X. K. *et al*. Highly crystalline macroporous β-MnO_2: hydrothermal synthesis and application in lithium battery. *Electrochim. Acta* **55**, 4915–4920 (2010).
38. Wang, G. L., Zhang, B., Wayment, J. R., Harris, J. M. & White, H. S. Electrostatic-gated transport in chemically modified glass nanopore electrodes. *J. Am. Chem. Soc.* **128**, 7679–7686 (2006).

Acknowledgements

This work is supported by the National Basic Research Program of China (Grant No. 2013CB922102 and 2011CB935800) and the National Natural Science Foundation of China (Grant No. 21071076, 21021062, and 51172106).

Author contributions

Q.L. and F.G. guided the entire project, carried out data analyses and co-wrote the manuscript. C.W. and H.P. performed the experiments, XRD characterization, SEM and TEM investigations. B.Z. and S.L. performed the experiments. All the co-authors discussed the results and commented on the manuscript.

Additional information

Supplementary information accompanies this paper at http://www.nature.com/scientificreports

Competing financial interests: The authors declare no competing financial interests.

How to cite this article: Wei, C.Z. *et al*. Two-Dimensional β-MnO_2 Nanowire Network with Enhanced Electrochemical Capacitance. *Sci. Rep.* **3**, 2193; DOI:10.1038/srep02193 (2013).